

PAPER • OPEN ACCESS

Vibration response analysis on the sand-wall collision

To cite this article: Li Yichen *et al* 2020 *J. Phys.: Conf. Ser.* **1550** 042043

View the [article online](#) for updates and enhancements.

You may also like

- [The time interval distribution of sand–dust storms in theory: testing with observational data for Yanchi, China](#)
Guoliang Liu, Lizhen Hao and Feng Zhang
- [Effect of abrasive particle hardness on interface response and impact wear behavior of TC17 titanium alloy](#)
Song-bo Wu, Zhen-bing Cai, Yu Lin et al.
- [SBOR: a minimalistic soft self-burrowing-out robot inspired by razor clams](#)
Junliang (Julian) Tao, Sichuan Huang and Yong Tang



ECS
The
Electrochemical
Society
Advancing solid state &
electrochemical science & technology

DISCOVER
how sustainability
intersects with
electrochemistry & solid
state science research

Vibration response analysis on the sand-wall collision

Li Yichen¹, Feng Kai², Jia Zongwen³, LiuGang^{1,4}, Wang Kai¹ and WangGang¹

¹ School of Petroleum Engineering, China University of Petroleum (East China), Qingdao 266580, China

² China Shipbuilding Institute 715, Hangzhou 310012, China

³ CNOOC Research Institute Co., Ltd. Drilling and Production Research Department, Beijing 100089, China

⁴ Author to whom any correspondence should be addressed.

Corresponding author's e-mail address, lg87323@126.com

Abstract. The real-time monitoring of solid particles in pipelines has been widely used in industry, especially during sand production in the petroleum industry. The monitoring result is determined by the vibration force response characteristics of sand-wall collision. In this paper, the process of the sand-wall collision was analyzed by Hertz contact theory, and the main vibration frequency from the sand-wall collision was calculated. The corresponding sand-wall impacting experiment was also investigated. Based on the theoretical and experimental research, the results showed that the main frequency of the sand vibration signal is inversely proportional to the diameter of the sand, and the initial velocity of the sand impact wall has little effect on the main frequency of the vibration signal. Besides, the sand-liquid film-wall experiment and simulation results showed that fluid viscosity little affect the stress transmission under low viscosity (less than 40 mPa·s), and the viscosity has the greatest effect on stress transfer under the high viscosity of 90 mPa·s. The above research lays the foundation for the detection ability of solid particles in pipe flow.

1. Introduction

The transportation of sand-carrying fluids in pipelines has attracted the attention of many industries^[1-3], such as chemical industry, metallurgy, mining, especially in the process of oil extraction^[4]. There are many hazards when sand enters the production pipeline. Sand entering the pipeline may cause equipment failure, affect the normal exploitation of the oil field and cause huge economic losses^[5, 6]. Therefore, real-time monitoring of sand particles is of great significance to optimize production and increase production capacity.

Sand production monitoring methods are divided into invasive monitoring methods and non-invasive monitoring methods^[7]. The intrusive monitoring method usually implants the probe inside the pipeline^[8]. However, this method is hysteretic and complicated to install. Therefore, the current non-implanted sand production monitoring technology is the main means to obtain oil well sand production information. However, the sand production signal is very weak compared to high-intensity background noise signals (such as fluid noise signals)^[9]. Therefore, research on the generation mechanism and characteristics of sand production signals can provide a basis for the collection and extraction of sand production signals.

In recent years, scholars have made some achievements in the study of the dynamic response characteristics of sand-wall contact-collision. Wang et al.^[10] experimentally studied the behavior of



particles hitting and rubbing a flat plate, and determined the wide-band response characteristics of particles to the flat plate impact force. Liu et al.^[11] experimentally studied the dynamic behavior of particle-plate interaction vibration. Mariella et al.^[12] found the influence of the size and velocity of sand particles on the distribution of the position of the impacted pipe wall. In summary, many scholars have obtained sand grain information through experimental research and various signal processing methods.

In this paper, the process of the sand-wall collision was analyzed by Hertz contact theory, and the main vibration frequency from the sand-wall collision was calculated. Besides, the influence of fluid viscosity on stress transfer was studied.

2. Sand particle-wall collision model

The vibration sensor collects signals using the relationship between the change in stress and acceleration^[13]. Therefore, the change in stress caused by the impact of sand particles on the pipe wall is an important factor affecting signal acquisition. Based on the Hertz contact theory, this section studies the process of particle-to-wall impact.

2.1. Theoretical equations

The assumptions of Hertz contact theory include the followings^[14]: the material is uniform, isotropic, and completely elastic. The friction force on the contact surface is negligible, and the surface is an ideally smooth surface. Antonyuk^[15] et al. studied the maximum contact stress of a spherical particle impacting a wall based on the Hertz contact theory. The contact schematic is shown in figure 1.

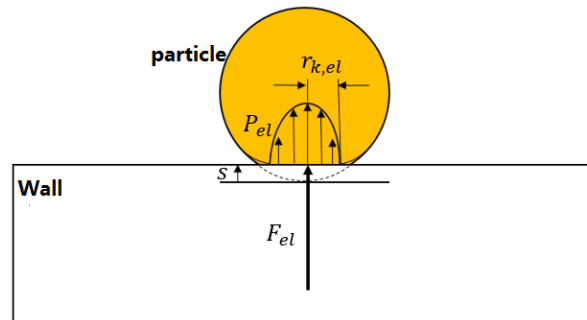


Figure 1. Schematic diagram of contact between sand and wall.

The elliptical pressure distribution equation in the circular contact region is shown in equation (1)^[15],

$$\left(\frac{P_{el}}{P_{max}} \right) = 1 - \left(\frac{r_k}{r_{k,el}} \right)^2, r_k \leq r_{k,el} \quad (1)$$

where P_{el} is the elliptical pressure distribution in the contact area, Pa; P_{max} is the maximum contact pressure, Pa; $r_{k,el}$ is the contact radius, m; r_k is the radius of the fully deformed area, m. Since the periphery of the contact pressure distribution will also be stretched, the radius of the fully deformed area is larger than the contact radius, $r_{k,max} \geq r_{k,el}$. Equation (1) is simplified,

$$P_{max} = \frac{3F_{el}}{2\pi r_{k,el}^2} \quad (2)$$

where F_{el} is the contact stress, N.

The formula for the maximum contact radius when the particle is in contact with the wall is shown in equation (3),

$$r_{k,el} = \left(\frac{3R^* F_{el}}{2E^*} \right)^{1/3} \quad (3)$$

where R^* is the equivalent radius of two contacts, m; E^* is the equivalent elastic modulus of two contacts, Pa. These two parameters can be calculated by equation (4),

$$\left\{ \begin{array}{l} R^* = \left(\frac{1}{R_1} + \frac{1}{R_2} \right)^{-1} \approx R_1 \\ E^* = 2 \left(\frac{1-\mu_1^2}{E_1} + \frac{1-\mu_2^2}{E_2} \right)^{-1} \approx \frac{2}{1-\mu_1^2} E_1 \end{array} \right\} \quad (4)$$

where R_1 is the particle radius and R_2 is the length of the wall. Since the particle radius is far smaller than the length of the wall, there is an approximate relationship, $R_1 \approx R$, $R_2 = \infty$. E_1, E_2 are the elastic modulus of the particles and the wall, Pa; μ_1, μ_2 are the Poisson's ratio of the particles and the wall, respectively.

Hertz proposed that the maximum stress at the contact center and the full elastic displacement are nonlinear,

$$F_{el} = \frac{2}{3} E^* (R^* s^3)^{1/2} \approx \frac{4}{3} \frac{E_1}{1-\mu_1^2} \left(\frac{d_1 s^3}{2} \right)^{1/2} = \frac{2}{3} E^* (R^*)^{1/2} s^{3/2} \quad (5)$$

where d_1 is the particle diameter, m; s is the complete elastomer displacement of the entire spherical particle caused by contact, m, $s = r_{k,el}^2 / R^*$.

According to the law of conservation of energy, when the impact velocity of a spherical particle reaches 0, the contact pressure at the center of the contact area is the largest impact stress in the entire impact process. Therefore, the maximum contact stress is shown in equation (6),

$$F_{el,max} = \left(\frac{125 m^*{}^3 E^*{}^2 R^*{}^6 v^6}{144} \right)^{1/5} \quad (6)$$

where v is the initial contact speed between the particles and the plate, m/s; m^* is effective mass, kg. The parameter can be calculated by equation (7),

$$m^* = \left(\frac{1}{m_1} + \frac{1}{m_2} \right)^{-1} \quad (7)$$

2.2. Vibration frequency of sand particle-wall collision process

The main frequency of the vibration signal generated by particles impacting the wall depends on the length of time that the particles contact the wall surface^[16]. The relationship between the two is as follows,

$$f = \frac{1}{T} = \frac{1}{2t} \quad (8)$$

where f is the main frequency of the particle impact, Hz; T is the total duration of the particle collision process, s; t is the length of time during which the particle and the wall contact the wall to undergo the maximum deformation, s. Therefore, to calculate the main frequency of the vibration signal of the particle impact wall, the static mechanical analysis of the impact process should be established.

According to Newton's third law, it has the following relationship,

$$\frac{\partial^2 \alpha}{\partial t^2} = \frac{dv}{dt} = -\frac{F_{el}}{m^{*2}} \quad (9)$$

where α is the normal overlap between the particles and the wall during the impact, m. Combined with formula (7), it is derived,

$$\frac{1}{2} d\left(\frac{d\alpha}{dt}\right)^2 = -\frac{4E^*(R^*)^{1/2} \alpha^{3/2}}{3m^{*3}} d\alpha \quad (10)$$

When the particles are just in contact with the wall, there is no overlap between the two, that is to say $\alpha=0, v=v_0$. v_0 is the initial velocity of the particle impacting the wall. When the wall deforms, and the particle and the wall have a certain overlap, the impact velocity of the particle is $\frac{d\alpha}{dt}$. When the overlapping part of the particle and the wall is the largest, the impact velocity of the particle is 0, and α reaches the maximum value α_{\max} . The parameter can be calculated by equation (11),

$$\alpha_{\max} = \left[\frac{15m^*}{8E^*} (R^*)^{-1/2} v_0^2 \right]^{5/2} \quad (11)$$

Integrate equation (10),

$$dt = \left[v_0^2 - \frac{8}{15m^*} E^* (R^*)^{1/2} \alpha^{5/2} \right]^{-1/2} d\alpha = v_0^{-1} \left[1 - \frac{8}{15m^* v_0^2} E^* (R^*)^{1/2} \alpha^{5/2} \right]^{-1/2} d\alpha \quad (12)$$

Let $x = \alpha/\alpha_{\max}$,

$$dt = \alpha_{\max} v_0^{-1} (1 - x^{5/2})^{-1/2} dx \quad (13)$$

During the particle's impact with the wall, α gradually increases from 0 to α_{\max} , which is gradually increased from 0 to 1. Therefore, the time from the impact of the particles on the wall to the maximum deformation is as follows,

$$t_{\max} = \alpha_{\max} v_0^{-1} \int_0^1 (1 - x^{5/2})^{-1/2} dx = 1.47 \alpha_{\max} v_0^{-1} \quad (14)$$

Therefore, the total contact time between the particles and the wall is as follows,

$$T = 2t_{\max} = 2.94 \alpha_{\max} v_0^{-1} \quad (15)$$

The calculation formula of the main vibration frequency of the particle impact wall is as follows,

$$f = \frac{1}{T} = \frac{1}{2t_{\max}} = \frac{1}{2.94 \left(\frac{5\pi\rho}{2E^*} \right)^{2/5} R^* v_0^{-1/5}} = \frac{v_0^{1/5}}{2.94 \left[\frac{5\pi(1-\mu_1^2)\rho}{4E_1} \right]^{2/5} R_1} \quad (16)$$

where E_1 is the elastic modulus of the sand particles, Pa. μ_1 is the Poisson's ratio of the sand particles, R_1 is the radius of the sand particles, and m . v_0 is the initial velocity of the sand impact contact, m / s.

3. Simulation study on the effect of fluid viscosity on stress transfer

In the sand-carrying flow, due to the existence of a liquid film on the pipe wall, when the sand particles impact the pipe wall, the oil film attached to the pipe wall is pressed by the sand particles and the pipe wall to generate pressure. In order to investigate the influence of fluid viscosity on the impact stress of particles, this section simulates the process of a single spherical particle squeezing a wall with a liquid film attached.

3.1. Governing equation

The physical model is shown in figure 2. A spherical particle is pushed by an external force to a flat wall with a certain thickness of liquid film on the surface.

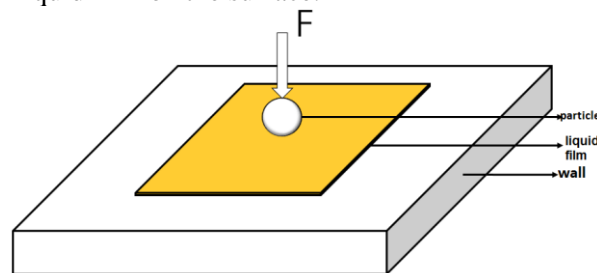


Figure 2. The wall covered by the liquid film is contacted by a spherical particle.

During the whole impact process, the particles hit the liquid film at a certain speed. In a certain impact time, the kinetic energy of the particles is converted into impact energy, and initial contact pressure is given to the liquid film. The maximum contact stress of the impact wall of the spherical particles in Section 2 is selected as the initial compression force f_i of the model.

$$f_i = \left(\frac{125m^3 E^2 R^* v^6}{144} \right)^{1/5} \quad (17)$$

3.2. Model construction and parameter selection

3.2.1. Geometric model. The scene in figure 2 is reduced to an equivalent model. Since the model is symmetric, a quarter of the above-mentioned geometric figure is simulated, as shown in figure 3. The fan shape is the part where the liquid film is located. The size of the part of the liquid film in the model is set to be extremely thin, and the remaining boundary is thinner, as shown in figure 4.

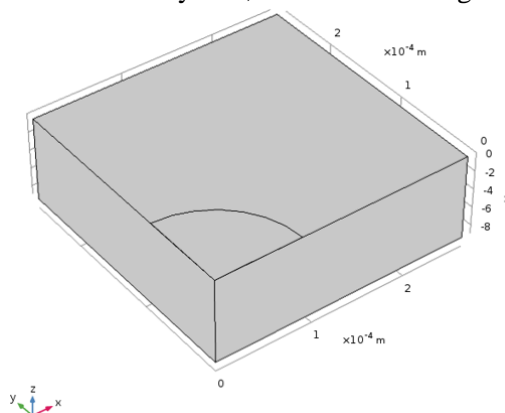


Figure 3. Schematic diagram of the geometric physical model.

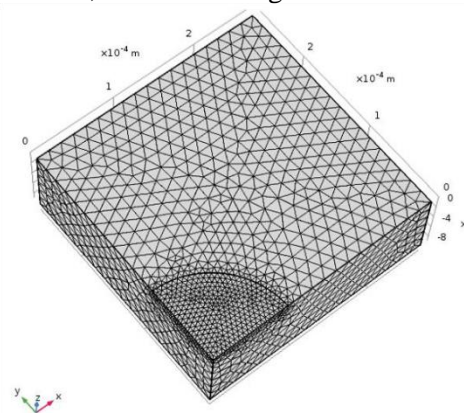


Figure 4. Schematic diagram of meshing.

3.2.2. *Parameter settings.* According to the indoor sand production experiment and field experience, the parameters of particle size, Poisson's ratio involved in the simulation were determined. It is shown in table 1. The particle mass, initial pressure and relative elastic modulus are calculated from equation (4), (7), and (17).

$$m = \frac{4}{3} \pi r^3 \rho = \frac{4}{3} \pi \times 0.000045^3 \times 2.65 \times 1000 = 1.01 \times 10^{-9} \text{ kg} \quad (18)$$

$$E^* \approx 2 \frac{E_1}{1 - \mu_1^2} = \frac{2 \times 6.22 \times 10^6}{1 - 0.2^2} = 1.296 \times 10^7 \text{ Pa} \quad (19)$$

$$f_i = \left(\frac{125 m^* E^* R^* v^6}{144} \right)^{1/5} = 1.26 \times 10^{-2} \text{ N} \quad (20)$$

Table 1. Model parameter setting.

Name	Expression	Description
r	$4.5 \times 10^{-5} \text{ [m]}$	Sand radius
Extent	r	Computer capacity
Force	$1.26 \times 10^{-2} \text{ [N]}$	Initial contact stress
b_0	$r/10$	Initial height of liquid film
Visc_mat2	$0.246 \text{ [Pa}\cdot\text{s]}$	Viscosity of liquid membrane (viscosity of oil)
Density_mat2	$860 \text{ [kg/m}^3\text{]}$	Density of liquid membrane (density of oil)
Time	$6 \cdot \pi \cdot \text{Visc_mat2} \cdot r^2 / \text{Force}$	Time scale
Nu_steel	0.28	Poisson's ratio of steel
E_steel	$2.05 \times 10^{11} \text{ [Pa]}$	Elastic modulus of steel
Density_steel	$7880 \text{ [kg/m}^3\text{]}$	Density of steel
E_eqv	$1.296 \times 10^7 \text{ [Pa]}$	Equivalent modulus of elasticity

4. Experimental setup

The vibration characteristics of sand particles in the process of pipe-flow transport and impact on the sand wall were studied by experiments.

4.1. Sand-wall collision experiments

This section will analyze the relationship between the characteristic frequency of the vibration signal characteristic of the gravel impact pipe wall and the gravel particle size, and the initial velocity of the gravel impact contact based on the gravel impact plate experiment.

4.1.1. *Experimental facility.* Select a steel plate made of SUS304 stainless steel and 9mm thick. A high-frequency vibration sensor is stuck in the center of one side of the steel plate, and the steel plate is fixed. A funnel is installed at a certain height directly above the center of the other side of the steel plate, which can ensure that the sand particles fall to the center position of the steel plate at a constant speed. In order to prevent the air flow from interfering with the trajectory of the sand particles, a glass tube is provided on the path where the sand particles descend. Place the steel plate obliquely to prevent the sand particles from falling in front from accumulating on the wall surface. The schematic diagram of the device is shown in figure 5.

4.1.2. *Experiment condition.* The experiments are mainly divided into two groups, including constant sand particle size and constant impact height. The specific experimental conditions are shown in table 2.

Table 2. Test conditions of the sand-wall collision.

Same size of sand		Same impact height	
Sand size (mesh)	Impact height (cm)	Sand size (mesh)	Impact height (cm)
50	20-100 with an interval of 20 cm	110-290 with an interval of 20 mesh	60

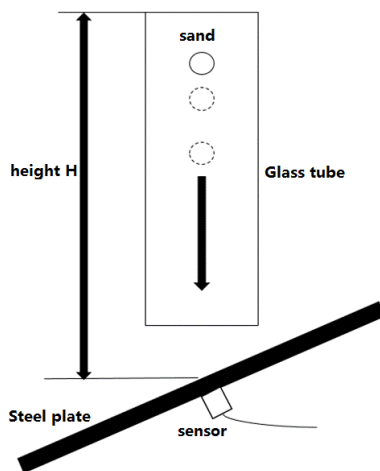


Figure 5. Schematic diagram of the overall design of the experimental bench.

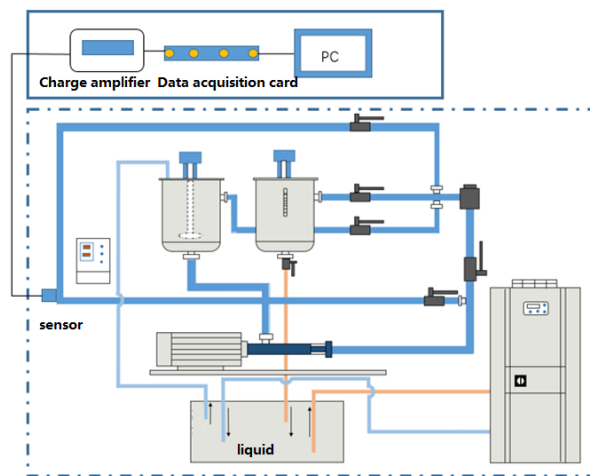


Figure 6. Schematic diagram of the liquid-solid two-phase indoor experimental platform.

4.2. Sand-carrying pipe flow transportation experiments

In this section, the relationship between fluid viscosity and vibration signal characteristics were obtained.

4.2.1. *Experimental rig.* A laboratory-scale sand-carrying flow-loop conveying system was constructed to simulate the sand-carrying fluid flow in a pipeline. Figure 6 shows the schematic representation of the test rig. The pipe used was a standard 304 steel model with a 25 mm nominal bore and an external diameter of 34 mm. The sensor was positioned in the outer wall of the exit of the elbow.

4.2.2. *Experiment condition.* The water-soluble tackifier (CMC) was mixed with water to the influence of viscosity changes on the vibration signal characteristics of sand particles impacting the pipe wall under the flow velocity. The experimental conditions are shown in table 3.

Table 3. Test conditions of the sand detection in sand-fluid pipe flow.

Sand size (mesh)	Flow velocity (m/s)	Sand concentration (wt.%)	fluid viscosity (mPa·s)
150	2	0.06	10-40 with an interval of 10

5. Results and discussion

5.1. The main vibration frequency of sand and wall collision

In Section 2, the main frequency calculation formula (16) of the particle impact wall is obtained by derivation. This equation shows that the main frequency of the particle impact wall vibration is related to many parameters of the particle, such as particle size, particle density, particle elastic modulus, and Poisson's ratio. In the sand production monitoring, the main physical quantities that change are the

velocity of the sand-carrying fluid and the particle size of the sand particles. Therefore, this section mainly considers the influence of these two factors on the dominant frequency of the sand plate impacting the plate vibration.

5.1.1. Theoretical calculation results. Use Equation (16) to calculate the normalized frequency of the vibration signal of the 150 mesh quartz sand impacting the wall at different heights of 10 cm to 100 cm with an interval of 10cm. And at 60cm impact height, the normalized frequency of vibration signals with different particle sizes was calculated. The calculation result is shown figure 7.

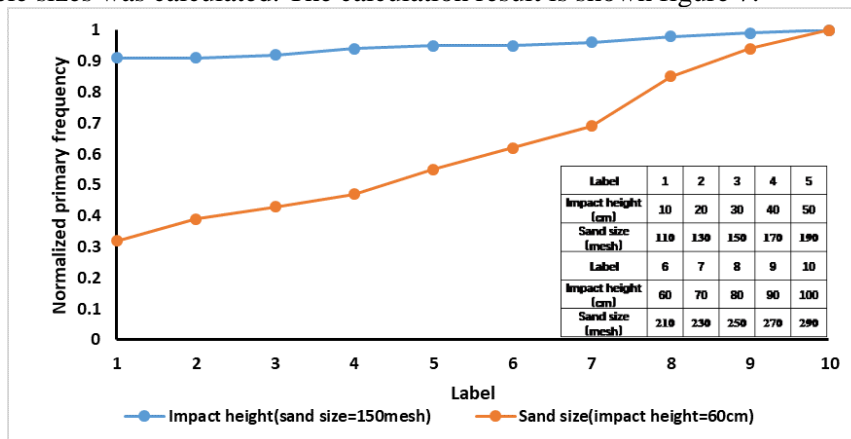


Figure 7. Main frequency relationship curve of particle impact wall.

It can be seen from figure 7 that with the decrease of the sand particle size, the normalized main frequency of the sand impact plate increases. As the impact height increases (the impact velocity increases), the normalized vibration frequency of the sand impacting the plate does not change much.

5.1.2. Analysis of vibration signal characteristics of different sand sizes. The short-time Fourier transform is used to analyze and study the non-stationary random vibration signals obtained from the test in section 4.1. Because the entire experimental system is in a non-closed state, the environmental noise in the low-frequency band and the inherent noise of the acquisition equipment have a greater impact on the experimental data, and the collected vibration signals need to be filtered. Figure 8 is a time-frequency three-dimensional spectrum diagram of the vibration signal of the sand particles impacting the flat plate after filtering.

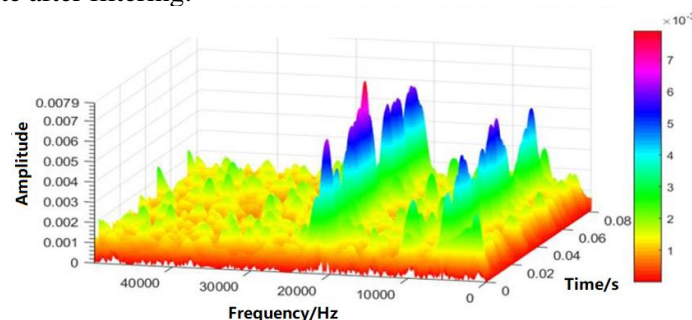


Figure 8. Three-dimensional spectrum of 150mesh /40cm shock signal STFT (after filtering).

It is obvious from figure 8 that there are two main frequencies of the collected vibration signals. The high frequency is around 22kHz and the low frequency is around 5kHz. According to previous research results, the impact of sand particles on the pipe wall is a high-frequency vibration signal^[17]. The low-frequency peaks in the three-dimensional spectrum diagram may be due to the frictional dominant frequency of the process in which sand particles slide from the center of the steel plate to the outside of the steel plate during the experiment. Therefore, the high-frequency part of the signal is selected for refined main frequency analysis.

It is difficult to determine the exact scale of the dominant frequency in the STFT three-dimensional time spectrum chart. Therefore, it is necessary to obtain the average value of the amplitudes of multiple frequency points at a specific resolution around 22kHz for comparison. Take 22kHz as the center, and select 10 frequency scale values at the interval of 100Hz forward and backward. Take the vibration signals of 150 mesh and 250 mesh sand particles at a height of 60cm as examples. Select the above 21 frequency points and make a section line for the frequency of 21-23kHz in the 3D time-spectrum diagram of STFT, as shown in figures 9 and 10.

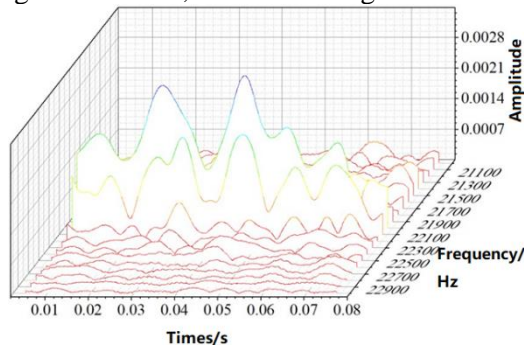


Figure 9. 21 frequency amplitude curves with time(150 mesh / 60cm).

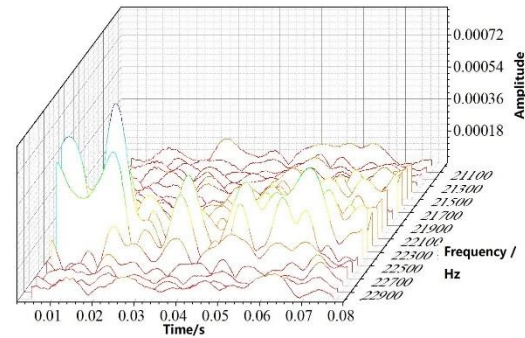


Figure 10. 21 frequency amplitude curves with time(250 mesh / 60cm).

Each profile curve in the figure represents the trend of the amplitude of a frequency point over time. For each amplitude curve, find the normalized amplitude average value over the entire time period, and draw a histogram, as shown in figure 11. The abscissa is 21 frequency points, and the ordinate is the average value of the frequency normalized amplitude over the entire time period.

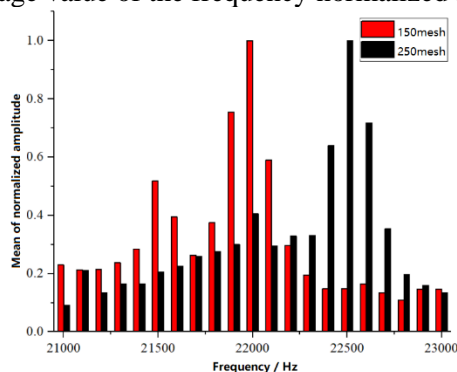


Figure 11. Normalized amplitude means histogram of 21 frequency points.

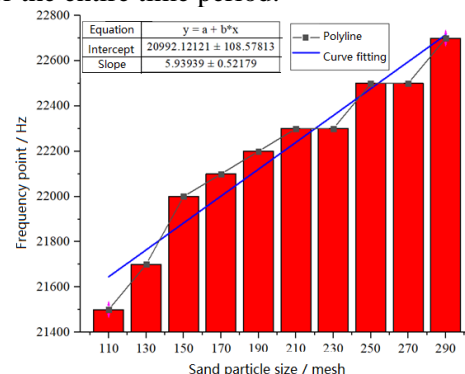


Figure 12. Relationship between the main frequency of impact signal and sand size.

It can be seen from the figure that when the sand particles with a size of 150 mesh are used to impact the wall with an impact height of 60 cm, the average amplitude of the 22 kHz frequency points is the highest among the 21 frequency points. When the sand with a particle size of 250 mesh hits the wall with an impact height of 60 cm, the average amplitude of the frequency of 22.5 kHz is the largest over the entire period. Therefore, the main frequencies of the vibration signals of 150-mesh gravel and 250-mesh gravel when impacting the steel plate at a height of 60cm are 22kHz and 22.5kHz, respectively.

Using the same analysis method, the main frequency fine-grained analysis is performed on the vibration signals obtained in the other eight groups of experiments, and figure 12 is obtained.

It can be seen from figure 12 that at the same impact height, the sand particles are impacted on the wall with 10 different sizes, and the main frequency of the vibration signal increases with the increase of the mesh of the sand (decreasing the particle size). Further, by fitting the relationship between them, it can be seen that they are approximately linear. This result is consistent with the conclusion of section 5.1.1.

5.1.3. *Analysis of vibration signal characteristics at different impact heights.* By using the same analysis method described above, the main frequency of the vibration signal of 150 mesh sand particles impacting the wall at different heights was analysed, and the histogram is drawn as shown in figure 13.

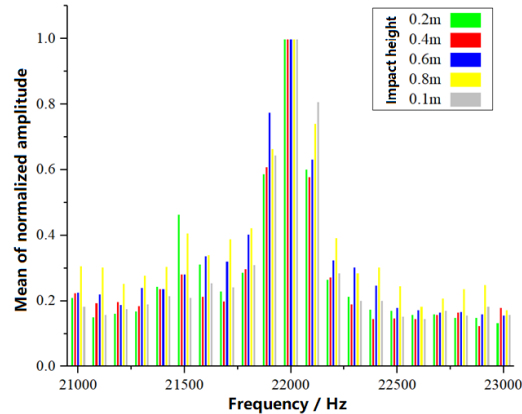


Figure 13. The relative average amplitude of each frequency at five impact heights.

When the 150-mesh sand impacts the plate at five different initial contact speeds, the highest point of the average amplitude of the frequency of the vibration signal appears at 22 kHz. In other words, it is considered that the initial contact speed of the gravel impact plate has no effect on the dominant frequency of the shock vibration signal, which is consistent with the conclusion in section 5.1.1.

5.2. The effect of fluid viscosity on stress transfer

In this section, simulation and experimental results are used to study the effect of fluid viscosity on the impact stress transmission of particles.

5.2.1. *Numerical simulation results.* A geometric physical model of the wall covering the liquid film is established in Section 3. It is used to study the influence of liquid film viscosity on the pressure distribution on the wall.

The simulated liquid film viscosity ranges from 1 to 246 mPa·s with a step size of 5 mPa·s. Record the maximum stress on the wall under different viscosities and draw a line diagram as shown in figure 14.

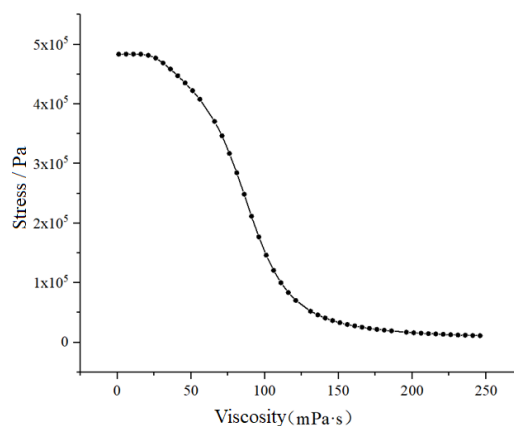


Figure 14. Liquid film viscosity and maximum stress.

Figure 14 shows the overall trend of the effect of liquid film viscosity on stress changes. That is to say, as the viscosity of the liquid film increases, the maximum contact stress generated by the particles hitting the wall decreases. Before the liquid film viscosity reaches 40mPa·s, the effect of the liquid film viscosity on the impact stress on the steel plate is very small, and the curve is relatively smooth. When the liquid film viscosity reaches 40-180mPa·s, the impact stress of the steel plate on the particles

decreases as the liquid film viscosity increases. At around 90mPa·s, the slope of the curve is the largest, and the effect of the viscosity of the liquid film on the stress distribution on the wall is most significant. After the liquid film viscosity reaches 180mPa·s, the impact stress on the steel plate hardly changes with the increase of its viscosity, and the curve tends to be horizontal.

5.2.2. Signal characteristics of vibrations of sand-carrying fluids with different viscosities on the wall. Through the experiments in Section 4.2, the high-frequency vibration sensor collected the vibration signal of the sand-carrying fluid impacting the pipe wall under the condition of the low-viscosity fluid. Select the NFFT length as 256, the window function as Hanning, and the window length as 127. Perform STFT analysis on the shock vibration signals of four fluids with different viscosities. Figure 16 is a two-dimensional time-frequency spectrum diagram with vibration signals at different viscosities.

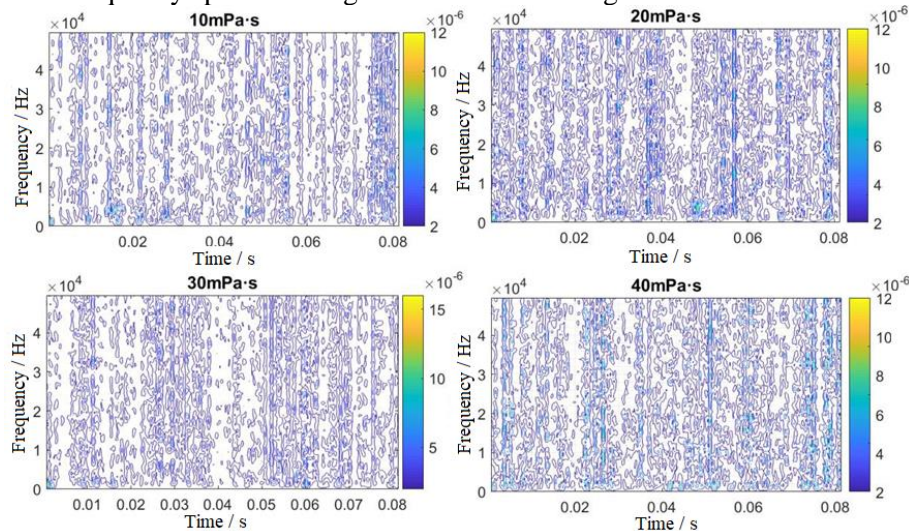


Figure 15. Comparison of STFT spectra under different viscosity conditions.

It can be seen from figure 15 that the frequency distribution of the four time-spectrum diagrams is uniform and the frequency amplitude of the shock signal of the liquid flow basically does not change with the change of the viscosity of the liquid flow. In other words, the impact force of the single-phase liquid flow on the pipe wall is not affected by the viscosity of the liquid flow. With the change of fluid viscosity, the impact energy of the tube wall is basically unchanged. This result is consistent with the simulation results in 5.2.1

6. Conclusions

Based on the Hertz theory, this paper analyzes the contact process of sand particles impacting the wall and derives the calculation formula of the vibration principal frequency of the process. The main frequency of the sand particle vibration signal is inversely proportional to its diameter through calculation. The initial velocity of sand has little effect on the dominant frequency of the sand particle vibration signal. The results of the laboratory test of the sand-wall contact also verified this conclusion. Besides, the sand-liquid film-wall experiment and simulation results showed that fluid viscosity little affect the stress transmission under low viscosity (less than 40 mPa·s), and the viscosity has the greatest effect on stress transfer under the high viscosity of 90 mPa·s.

At present, real-time sand production monitoring technology based on sand production signal collection and analysis is one of the main means to obtain sand production information from oil wells. Through theoretical calculation, simulation analysis, and experimental verification, the characteristics of several important parameters affecting the real-time monitoring of sand production are obtained in this paper, which lays the foundation for the establishment of a sand production calculation model based on the characteristics of the vibration signal of the wall impacted by sand particles.

Acknowledgments

This paper was supported by the Project (CCL2018RCPS0044RNN).

References

- [1] Ranjith P, Perera M, Perera W, Choi S and Yasar E 2014 Sand production during the extrusion of hydrocarbons from geological formations: A review *J Petrol Sci Eng.* **124** 72-82
- [2] Wang Z-Z, Tian H, Deng J-G, Tang S-B and Shi L-J 2006 Improving well productivity through sand management *Production Technology.* **28**(3) 59-63
- [3] Boyd JW and Varley J 2001 The uses of passive measurement of acoustic emissions from chemical engineering processes *J Chemical Engineering Science.* **56**(5) 1749-67
- [4] Wang K, Liu Z, Liu G, Yi L, Yang K, Peng S and Chen M 2015 Vibration sensor approaches for the monitoring of sand production in Bohai bay *Shock Vib.* **2015**
- [5] Jackson S, Gundemoni B and Barth P, editors. Sand control in corrosive and erosive downhole conditions at high temperatures. SPE Asia Pacific Oil & Gas Conference and Exhibition; 2016: Society of Petroleum Engineers.
- [6] Zamani M, Seddighi S and Nazif HR 2017 Erosion of natural gas elbows due to rotating particles in turbulent gas-solid flow *J Nat Gas Sci Eng.* **40** 91-113
- [7] Yan C, Zhai L-S, Zhang H-X, Wang H-M and Jin N-D 2017 Cross-correlation analysis of interfacial wave and droplet entrainment in horizontal liquid-liquid two-phase flows *Chem Eng J.* **320** 416-26
- [8] Kesana N, Throneberry J, McLaury B, Shirazi S and Rybicki E 2014 Effect of particle size and liquid viscosity on erosion in annular and slug flow *Journal of Energy Resources Technology.* **136**(1) 012901
- [9] Wang K, Liu G, Li Y, Wang J and Wang G 2019 Non-intrusive characterization of sand particles dispersed in gas-water bubbly flow using straight and bent pipes with vibration sensing *Powder Technol.* **344** 598-610
- [10] He L, Zhou Y, Huang Z, Wang J, Lungu M and Yang Y 2014 Acoustic analysis of particle-wall interaction and detection of particle mass flow rate in vertical pneumatic conveying *Ind Eng Chem Res.* **53**(23) 9938-48
- [11] Ma Y, Liu M, An M and Xu X 2017 Experimental investigation of collision behavior of fluidized solid particles on the tube wall of a graphite evaporator by vibration signal analysis *Powder Technol.* **316** 303-14
- [12] Leporini M, Terenzi A, Marchetti B, Corvaro F and Polonara F 2019 On the numerical simulation of sand transport in liquid and multiphase pipelines *J Petrol Sci Eng.* **175** 519-35
- [13] Wang K, Liu Z, Liu G, Yi L, Chen M, Peng S, He J, Zhao W and Zhao G 2014 Research on Frequency Response Based on Piezoelectric Accelerometer *Measurement & Control Technology.* **33**(9) 116-9
- [14] Machado M, Moreira P, Flores P and Lankarani HM 2012 Compliant contact force models in multibody dynamics: Evolution of the Hertz contact theory *Mech Mach Theory.* **53** 99-121
- [15] Antonyuk S, Heinrich S, Tomas J, Deen NG, van Buijtenen MS and Kuipers J 2010 Energy absorption during compression and impact of dry elastic-plastic spherical granules *Granular Matter.* **12**(1) 15-47
- [16] Xie J. Study on the dynamic characteristics of micro-scale particles impacting the surface of a flat plate: Dalian University of Technology; 2017.
- [17] Wang K, Liu G, Li Y, Qin M, Wang J, Wang G and Mei DJPt 2019 Vibration and acoustic signal characteristics of solid particles carried in sand-water two-phase flows *Powder Technol.* **345** 159-68